 CMES, vol.87, no.6, pp.530-555, 2012

AFM and Nanoindentation Studies of Bone Nodules on Chitosan-Polygalacturonic Acid-Hydroxyapatite Nanocomposites

R. Khanna[1,2], **D. R. Katti**[1] **and K. S. Katti**[1]

Abstract: Here we report a new *in situ* nanoindentation technique developed to evaluate the composite mechanical behavior of cell-biomaterial construct under physiological conditions over the time scale of bone nodule generation. Using this technique, mechanical behavior of osteoblast cell-substrate interfaces on tissue engineered materials (chitosan-polygalacturonic acid-nanohydroxyapatite (CPH) films) is investigated. Mechanical behavior of cells in the elastic regime over the time scale of cell adhesion (1 day), proliferation (4 days), development (8 days) and maturation (22 days) of bone nodules is evaluated. Our results indicate that the elastic properties of flat cells are higher (indicating stiffer response, after 4 days, as compared to the round cells after 1 day and oriented cells after 8 days. Elastic properties of cells ($\sim$5-12 MPa), soaked CPH films ($\sim$10-20 MPa) and that of cell-CPH composites ($\sim$3-9 MPa) fall in the same order of magnitude. A similar range of elastic properties of cell-CPH composites are measured over time, implying that unique interactions between cells and CPH films are maintained that may provide a favorable mechanical environment to growing cells and bone nodules. Atomic Force Microscopy (AFM) imaging studies on individual cells reveal that the cells respond to local changes in substrate topography (as a result of substrate swelling) by modulating their shapes and various focal adhesions. Overall, CPH films provide a favorable microenvironment for cell organization and bone nodule regeneration that regulates the mechanical behavior of cell-substrate interactions.

Keywords: nanoindentation, mechanical behavior, cell-substrate indentation, tissue engineering.

[1] Department of Civil Engineering, North Dakota State University, Fargo ND 58105
[2] work performed at NDSU, Currently at Department of Biomedical Sciences College of Life and Health Sciences JSPS fellow, Chubu University

1 Introduction

Tissue engineering attempts to repair or regenerate damaged tissue by using an engineered scaffold material system that favors cell adhesion, proliferation, differentiation and organization to develop healthy tissue while the scaffold degrades (Engelmayr et al. 2008; Freed et al. 2009; Khanna et al. 2011b; Langer & Vacanti 1993; Wei & Ma 2008). Engineering an osteoinductive nature to the scaffold requires replication of the favorable local environment of native bone. Moreover, an appropriate mechanical environment of scaffold is required to regenerate healthy bone. Several advanced tissue engineering strategies have been used to develop scaffolds with mechanical properties similar to native tissues (Engelmayr et al. 2008; Freed et al. 2009; Pagliari et al. 2011; Rezwan et al. 2006) Many polymer scaffolds developed till now do not fulfill the mechanical property requirements for bone regeneration and as a result, either scaffolds exhibit inadequate mechanical properties or exhibit limited ability to stimulate bone regeneration. One effective tissue engineering strategy to mimic the mechanical environment of native bone is engineering the mechanical properties of tissue engineered constructs to match the biomechanical characteristics of native bone. Current materials design strategies include the use of hydroxyapatite in conjunction with several synthetic and natural biodegradable polymers (Gaharwar et al. 2011; Verma et al. 2006a; Verma et al. 2008a, 2009; Verma et al. 2008b) to induce mineralization (Ambre et al. 2011; Katti et al. 2010b; Nudelman et al. 2010; Verma et al. 2006b; Verma et al. 2010) regeneration of hierarchically organized bone's extracellular matrix (ECM) (Khanna et al. 2011b) as well as use of artificial ECMs (Lutolf & Hubbell 2005) and has shown significant improvement in mechanical properties by biomimetic means (Katti et al. 2006b; Verma et al. 2008b) In addition, the versatility in properties of hydrogels have led to their widespread use in several biomedical applications (Allan S 2002; Banwell et al. 2009) including tissue engineering (Du et al. 2008; Slaughter et al. 2009; Wheeldon et al. 2010) and bone regeneration (Abrahamsson et al. 2010; Gkioni et al. 2010; Khanna et al. 2011b; Verma et al. 2010).

In the field of bone tissue engineering, measurement of elastic properties of proliferating and differentiating cells, and the developing bone nodules on biodegradable constructs is useful. This evaluation is the focus of the present study, in addition to the evaluation nanomechanical elastic properties of cell-biomaterial interfaces over the time scale of cell adhesion, proliferation and tissue regeneration as material degrades. Nanoindentation is a depth sensing technique and has been used to evaluate the mechanical properties of various engineering materials, (Basu & Barsoum 2007; Oliver & Pharr 1992, 2004, 2010; Pharr & Oliver 1992; Rho et al. 1999; Saha & Nix 2002) yeast cells, (Arfsten et al. 2008) mineralized and soft tissues, (Balooch et al. 2008; Ebenstein & Pruitt 2004; Ebenstein & Pruitt 2006; Roy et al.

1999) biological composites, (Katti et al. 2006a; Mohanty et al. 2006) and dental materials (Balooch et al. 2004; Kinney et al. 2003) Analysis of local mechanical properties of biological systems have also been carried out using Atomic Force Microscopy (AFM) and indentation methods to evaluate the changes in properties over time for chondrocytes (Ng et al. 2007) stem cells, (Darling et al. 2008; Tai et al. 2008; Yim et al. 2010) and also for understanding tissue physiology, disease progression, wound healing processes and cell-matrix interactions (Discher et al. 2009; Guilak et al. 2009; Ingber 2003; Subra 2007; Van Vliet et al. 2003; Wang et al. 1993).

Experimental set up, testing methodology and results of nanoindentaion tests on live osteoblasts and osteoblasts-tissue culture polystyrene composites have been described in our prior work. (Khanna et al. 2011a) In this work, biodegradable and biocompatible biopolymers (chitosan and polygalacturonic acid) and nanohydroxyapatite particles are used to prepare CPH films to mimic bone's extracellular matrix (ECM). *In vitro* bone nodules were found in absence of osteogenic supplements, thereby suggesting osteoconductive and osteoinductive properties of CPH films and scaffolds (Khanna et al. 2011b; Verma et al. 2010) In addition, our previous studies (Khanna et al. 2011b) indicate that the micro and nanostructure of the bone nodules reveal a hierarchical structure mimicking natural bone (mineralized collagen fibers and fibrils) as well as chemistry of the natural bone. CPH films showed swelling characteristics in cell culture media over 48 days as shown by changes in the physico-chemical-mechnical characteristics of the films (Khanna et al. 2010) The specific objectives of this work were to perform *in situ* nanoindentation experiments on dry, soaked (w/o cells) and cell-seeded CPH nanocomposites using *in situ* nanoindentation technique. *In situ* nanomechanical experiments on soaked and cell-seeded samples were performed over the time scale of initial cell adhesion (1 day), proliferation (4 days), developing bone nodule (8 days) and bone nodule formation (22 days), respectively. Topographical changes in cellular morphology were analyzed after one day and after two days cell-seeded CPH films by contact mode AFM.

2 Experimental

2.1 Materials used and CPH nanocomposite film synthesis

Chitosan (MW 190,000, $>$85 % deacetylation) and polygalacturonic acid (MW 25000) were obtained from Sigma-Aldrich chemicals, USA. Disodium hydrogen phosphate (Na_2HPO_4), an ultrapure bioreagent, was obtained from J.T. Baker, USA. Calcium chloride ($CaCl_2$) GR grade, was obtained from EM Sciences, USA. TCPS petridishes were procured from BD Biosciences, USA. HAP nanoparticles

were prepared by wet chemistry route from Na_2HPO_4 and $CaCl_2$. The detailed processing route is reported elsewhere (Katti et al. 2006c). CPH nanocomposite films were made using chitosan, and polygalacturonic acid biopolymers and HAP nanoparticles. Briefly, CPH nanocomposite films were prepared at a concentration of 1g/100 ml with deionized water (DI) and 20 % sonicated solution of HAP nanoparticles. Films were deposited directly onto TCPS petri dishes. Detailed film synthesis route is described elsewhere .( ) (Khanna et al. 2011a; Khanna et al. 2011b).

2.2 Cell culture experiments

Human osteoblasts (hFOB 1.19; CRL 11732; ATCC) were cultured and expanded in Dulbecco's Modified Eagle Medium (DMEM/F12; Hyclone), supplemented with 2.5 mM l-glutamine (without phenol red), 10 % fetal bovine serum (FBS; ATCC) and 0.6 mg/ml antibiotic (G418; J R Scientific Inc.). Samples were UV-sterilized for 1 h under biohazard safety hood, seeded with a cell density of 2×10^4 cells/cm^{2}and placed under standard cell culture conditions (37^{o}C, 5 % CO_2) in a humidified atmosphere. At the end of predetermined time, cell-seeded samples were taken out of incubator, washed 2X with PBS to remove unattached cells and by-products of cells and CPH samples. Prior to live cell indentation experiments, representative optical micrographs were recorded using an inverted microscope (Axiovert CFL model, Carl Zeiss). Cell viability was assessed by trypan blue exclusion, was $>$90%. The hFOBs used in the experiments were between passages 6-9. Fresh media was added to cell seeded samples every 4 days.

2.3 Atomic force microscopy (AFM)

AFM was employed to determine the cell morphology, and topography of soaked CPH nanocomposite films. Contact mode AFM (multimode AFM: Veeco Metrology Group, Santa Barbara, CA), equipped with a Nanoscope IIIa controller and J-type piezoscanner was used with silicon nitride cantilever probes (Model: NP-S20) with a nominal stiffness of 0.06 N/m. Size, morphology, topography and subsurface topographic features of cell and CPH nanocomposite films were obtained by high resolution height and deflection images, respectively. Briefly, cell-seeded CPH nanocomposite film (1 day and 2 days cultured) samples were washed 2X with PBS and fixed with 2.5% glutaraldehyde for 6 h at room temperature. Cells and bone nodule samples were imaged in a fully hydrated environment (cell culture fluid; 37^{o}C) using fluid cell set up (Veeco Metrology, CA).

2.4 In situ nanomechanical testing of cells and cell-CPH composites

Displacement controlled nanoindentation experiments on dry, soaked and cell-seeded samples were performed with Berkovich diamond indenter fluid tip (three-sided pyramidal; 100-200 nm tip radius) using Hysitron Triboscope nanomechanical instrument (Minneapolis, MN) equipped with multimode AFM (nanoscope IIIa controller and J-type piezo scanner system) (Veeco Metrology, Santa Barbara, CA). Details about experimental set up with custom designed fluid cell, 37^oC heating stage and protocols for performing the temperature controlled *in situ* live cell nanoindentation tests have been given elsewhere (Khanna et al. 2011a). Briefly, cell seeded samples were glued inside the fluid cell and flushed with cell culture medium. Subsequently, samples were placed onto nanoindentation sample stage and the whole tip-sample-fluid assembly was heated and maintained at 37^oC for about 20 minutes for thermal equilibration to maintain physiological test conditions. These kinds of environment and temperature-controlled nanoindentation experiments have been referred as '*In situ* conditions', in this manuscript. Extreme care was taken to keep the samples completely immersed for the entire duration of experiments. In this work, a novel cell-substrate indentation experiment was designed in which the indenter tip causes large deformations (in excess of several 100s of nanometers) that yield the composite nanomechanical response from both the cell and underlying substrate, as shown in the schematic (figure 1). Sectional views of Berkovich indenter tip-cell-CPH film-TCPS substrate are shown schematically. Schematic describes that at a particular depth, indentation responses can be obtained from various regions of cell-substrate composites, depending on the position of indenter tip. *In situ* cell and cell-substrate indentation experiments were performed at maximum indentation depths of 1000, 2000, 3000, and 4000 nm, respectively, at loading and unloading rate of 100 nm/s.

Dry substrates were indented at maximum indentation depths of 40, 100 and 500 nm with a loading-unloading rate of 10 nm/s, respectively. Soaked CPH films were indented at indentation depths of 500, 1000 and 2000 nm with loading and unloading rate of 100 nm/s. Low depth indentations did not result in good LD curves due to very soft nature of surfaces of swollen CPH substrates. A triangular loading function was used for all the nanoindentation experiments as also reported for nanoindentation compression testing on single yeast cells (Arfsten et al. 2008; Mashmoushy et al. 1998).

In a typical experimental routine, an indenter tip approaches the sample surface with a force of 3 μN, while keeping the scan size to zero. After tip is engaged onto the sample surface, the contact force is immediately changed to 0.75 μN. A special nanoindentation test procedure was adopted to get varying mechanical responses within the cells and cell-substrate composite bodies. Briefly, once the indentation

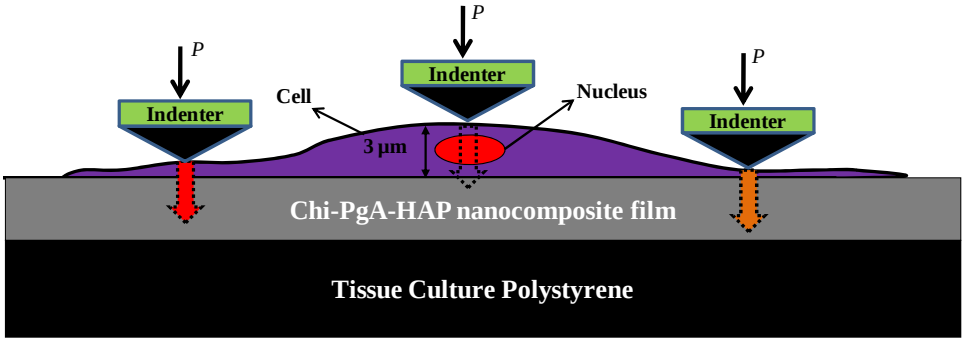

Figure 1: Sectional view of Berkovich indenter tip-cell-substrate, showing the schematic view of cell-substrate indentations on a single cell attached onto Chi-PgA-HAP film deposited onto TCPS substrate; Dotted arrows pointing downwards indicate the amount of deformation applied (P) onto cell-substrate construct to yield composite responses of cell and CPH film.

response from the cell was identified, same cell was stressed again to a deeper penetration depth without changing the position of indenter tip to get the mechanical responses from bulk regions of the cell. Repeated loading and unloading cycles were performed on cells to ensure the repeatability and reproducibility of the indentation tests. Spacing between the indents was varied from 30-80 μm. All the experiments on cell-seeded substrates were completed within 2 hours.

2.5 Analysis of L-D Data

Load-displacement curve of each test was carefully analyzed to separate cell indentation and cell-substrate indentation responses. Composite cell-substrate indentation response was identified by drawing tangents along the initial linear portion of loading curve and any deviation from tangent line was recorded as a measure of change in loading slope/stiffness. Contact stiffness was calculated by applying power-law fit to initial unloading portion of load-displacement curve and analytically differentiating the power-law relation, following Oliver-Pharr method (Oliver & Pharr 1992). Reduced modulus was calculated from the stiffness and contact area measurements using Hysitron analysis software. Elastic modulus for each indent was further determined from reduced modulus and is given by the following relation.

$$\frac{1}{\mathrm{E}_r} = \frac{1-\nu_s^2}{\mathrm{E}_s} + \frac{1-\nu_i^2}{\mathrm{E}_i}$$

Where, E_r=reduced elastic modulus; E_s=elastic modulus of sample; E_i=elastic modulus of indenter; ν_i=Poisson's ratio of indenter; ν_s=Poisson's ratio of sample. In this work, elastic modulus of 1141 GPa and Poisson's ratio of 0.07 were used for the diamond indenter tip. Poisson ratio of 0.5 was used for calculation of elastic moduli of biological cells as also commonly in literature (Darling et al. 2008; Ng et al. 2007) The CPH film display hydrogel-like swelling behavior and Poisson's ratio of 0.5 has been reported under immersed conditions in physiological fluids .(Ahearne et al. 2005). In this work, all the experiments are performed under fully immersed conditions. Therefore, a Poisson's ratio of 0.5 has been chosen to obtain the elastic moduli of soaked CPH films.

It should be noted that Oliver and Pharr method was initially developed for hard elasto-plastic materials (Oliver & Pharr 1992) and neglects viscous effects that are likely to be important for deformations under large strains/longer duration test conditions. It may lead to some differences in absolute values of cell/substrate moduli reported in this work. In addition, indentation data representing substrate effects due to stiff TCPS were excluded from the data analysis. TCPS substrates were only used as a support for deposition of CPH films.

For all the dry, soaked and cell-seeded samples, at least 30 indents were made under each set of experimental conditions. All the experiments were repeated at least 3 times on triplicate samples to ensure repeatability and reproducibility. To be noted here that standard deviation calculations are often made to show the experimental error in measurement. In this work, at a particular depth, variation in elastic properties arise due to presence of different constituents (such as cells and CPH film) possessing different physical/biological characteristics thereby, expect to exhibit their unique mechanical behavior. Under such a scenario, a range of modulus values were plotted to indicate the difference in elastic properties of cells and cell-CPH composites.

3 Results

3.1 Cellular response on biodegradable CPH films: AFM topography

Figure 2a shows a typical AFM height image (31 μm $\times$ 31 μm) of dry CPH nanocomposite film, indicating presence of randomly distributed CP fibers ($\sim$1-2 μm in diameter). The average particle size of HAP nanoparticles was found to be $\sim$50 nm (Khanna et al. 2009). The sectional profile in figure 2b shows the height distribution of surface asperities on dry CPH film. Figure 2c shows a typical AFM height image (90 μm $\times$ 90 μm) of cellseeded CPH film after 1 day of culture. Cells appear to lie flat onto the fibrous CPH microstructure and exhibit maximum cell height of $\sim$1.25 μm as shown on the sectional profile. Topographic

variations in fibrous nanocomposite microstructure and cell surface topography are shown by sectional profile (figure 2d) Substantial changes in cellular responses and substrate topography after 2 days of culture are typically shown by AFM height and deflection images (31 μm $\times$ 31 μm) (figure 2e and figure 2g) and sectional profile (figure 2f). Interestingly, a unique cell morphology is observed after 2 days of culture. Several long filapodia are observed from cell periphery and spread over several μm on CPH film substrate. Sectional profile (figure 2f) shows a maximum depth of $\sim$600 nm inside the front edge of cell at $\sim$15 μm regions as shown by dotted line suggesting that cell has taken the shape of grooves. Observation of sample surface shows presence of sharp ridges, valleys and grooves indicating that substrate topography is changed after 2 days of culture. AFM deflection image (figure 2g) clearly reveals the sub-surface features of cell and $\sim$300-400 nm filapodia protruding on the sample surface.

3.2 In situ nanomechanical properties of dry and soaked CPH films

Nanoindentation experiments on soaked CPH films are performed under *in situ* conditions (cell culture fluid; 37^{o}C) to closely simulate the physiological conditions.The nanomechanical elestic properties of dry CPH films are obtained with displacement control experiments at depths of 40, 100 and 500 nm with constant loading and unloading rate of 10 nm/s. Elastic moduli of CPH films at 40 nm indentation depth is observed to be $\sim$10-33 GPa. A spread in elestic modulus (E) indicates the nanomechanical property of individual constituents of CPH films consisting of soft polymeric (lower range of E) and stiffer HAP (higher range of E) materials. Mid-range of elastic moduli values result from CPH composite response. At higher indentation depths, substrate effects are observed due to presence of stiff TCPS substrate lying underneath the CPH films.

CPH films swell in cell culture media (Khanna et al. 2010) and it is possible to perform indentations at higher depths of 1000, and 2000 nm, respectively at loading and unloading rate of 100 nm/s. *In situ* nanoindentation tests were performed on soaked CPH films for soaking durations of 1, 4, 8 and 22 days, respectively. Selected nanoindentation data obtained at 1000 nm depths is described here. The modulus of soaked CPH films after 1 day ($E_{Soaked\ CPH,\ 1\ day}$) is observed to be 7.7-20.9 MPa, after 4 days ($E_{Soaked\ CPH,\ 4\ days}$), 8.5-21.5 MPa, after 8 days ($E_{Soaked\ CPH,\ 8\ days}$), 10.8-22.8 MPa and after 22 days ($E_{Soaked-CPH,\ 22\ days}$), 7.5-18 Mpa respectively. A significant decrease in elastic moduli of soaked CPH films was not observed over 22 days of soaking in cell culture media. A similar trend in elastic properties was obtained at other indentation depths as well.

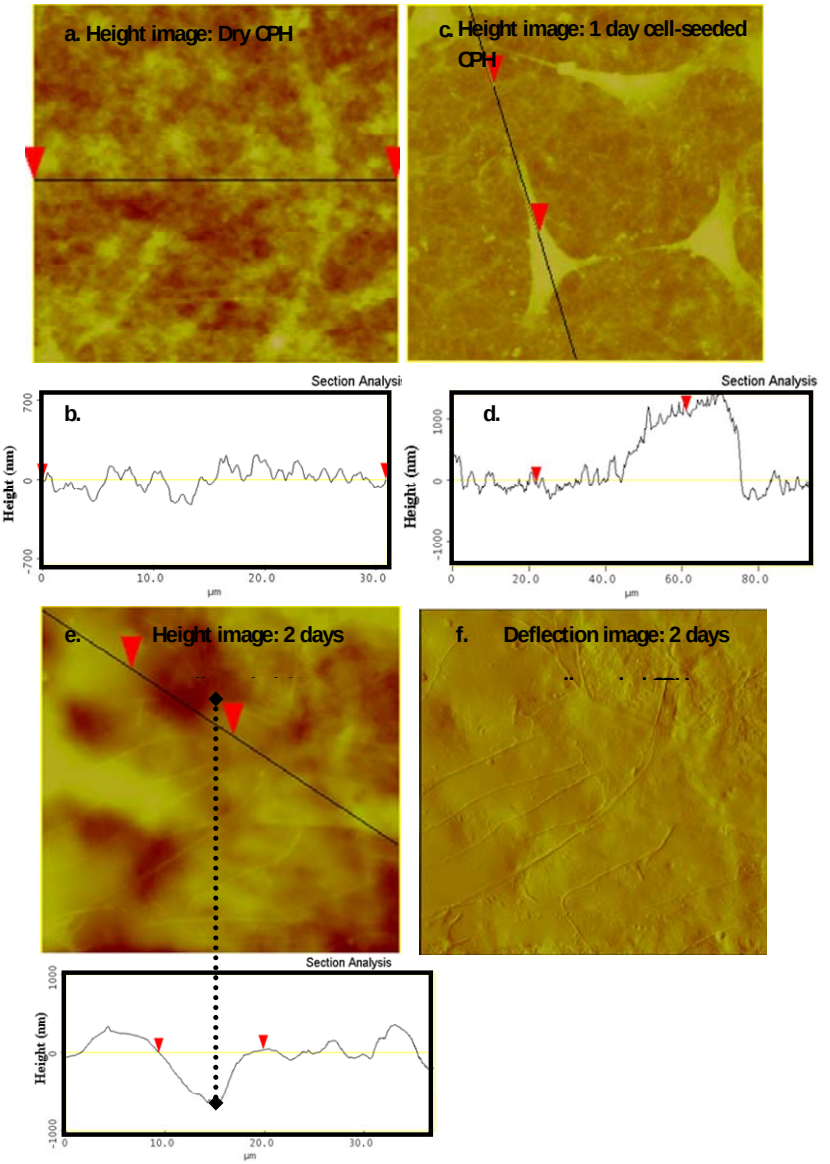

Figure 2: AFM analysis on dry and cell-seeded CPH films after 1 day and 2 days of culture. Surface topography of dry CPH film is shown by height image (a,c) and sectional analysis (b.d). AFM height images (c) and sectional analysis (d) show flat cell morphology of 1 day cultured cells; after 2 days of culture, several uneven grooves and ridges are observed in substrate topography and unique cellular response is shown by filapodia extension over several micrometers on CPH substrate, as shown in AFM height image (e) and sectional analysis (g). Dotted line points to the front edge of the cell which is observed to be spread into $\sim$600 nm groovy surface. Sub-surface features of cells and filapodia are revealed by deflection image (g).

3.3 in situ nanomechanical experiments on live osteoblasts and osteoblast-CPH composites over time

3.3.1 In situ nanomechanical studies of cells and cell-CPH composites after 1 day of culture.

Figure 3a shows a schematic representation of cells attached onto CPH film during the initial cell adhesion phase. Optical micrograph of 1 day cell-seeded CPH film shows the presence of smaller sizes (up to 40 μm) of the cells representing an initial cell adhesion phase (figure 3b). The smaller sizes are expected in early stages of cell adhesion wherein, cells are yet to flatten out on substrate and thus appear larger. The small 'spiky' features observed are the salt particles in the cell culture medium. Representative load-displacement (LD) curves on cells obtained at depths of 1000 nm and 2000 nm depth are shown in figure 3c. The shape of the LD curves indicates reversible cell deformation suggesting that cells recover their shape on unloading. LD curves obtained at 3000 nm and 4000 nm indentation depths (figure 3d) represent the composite mechanical response of cell and underlying CPH film substrate, as shown by increased stiffness. The increased stiffness (change) is described as evidence of initiation of composite response. LD curves obtained at higher depths are also reversible but display large hysteresis as compared to low depth indentations. *In situ* elastic moduli of cells and cell-CPH composites at a particular depth are shown by vertical bars in figure 3e-h. Elastic moduli of cells at 1000 nm depth are in the range of 5.3-12.0 MPa and represent indentation response from top layers of cell surface mainly, the membrane and cytoskeleton structures. Unique mechanical behavior of cells are observed at depths of 2000 nm i.e. $E_{Cell-A,\ 2000\ nm}$= 1.7-2.5 MPa, and $E_{Cell-B,\ 2000\ nm}$= 3.7-5.9 MPa. Bulk elastic moduli of cells are measured at 3000 nm depths ($E_{Cell,\ 3000\ nm}$= 1.1-2.3 MPa). Elastic moduli of cell-CPH composites at 3000 nm ($E_{Cell-CPH\ composite,\ 3000\ nm}$) is found to be 3.3-8.0 MPa, and 1.6-6.6 MPa at 4000 nm ($E_{Cell-CPH\ composite,\ 4000\ nm}$). The inherent heterogeneity in the cellular internal structure can lead to a variation in elastic moduli of cells. Varying thickness of cell-CPH composite layers under the indenter tip can result in a spread in elastic moduli of cell-CPH composites.

3.3.2 In situ nanomechanical characterization of osteoblasts and osteoblasts-CPH composites after 4 days of culture.

Figure 4a shows a schematic representation of flat cells, and cell-cell interactions on CPH films with an increase in cell culture time to about 4 days. Figure 4b shows a typical optical micrograph of cells attached onto CPH film after 4 days of culture. Changes in cellular responses are suggested to result from cell clustering, indicating cell assemblage and organization over time. Both flat and round cells

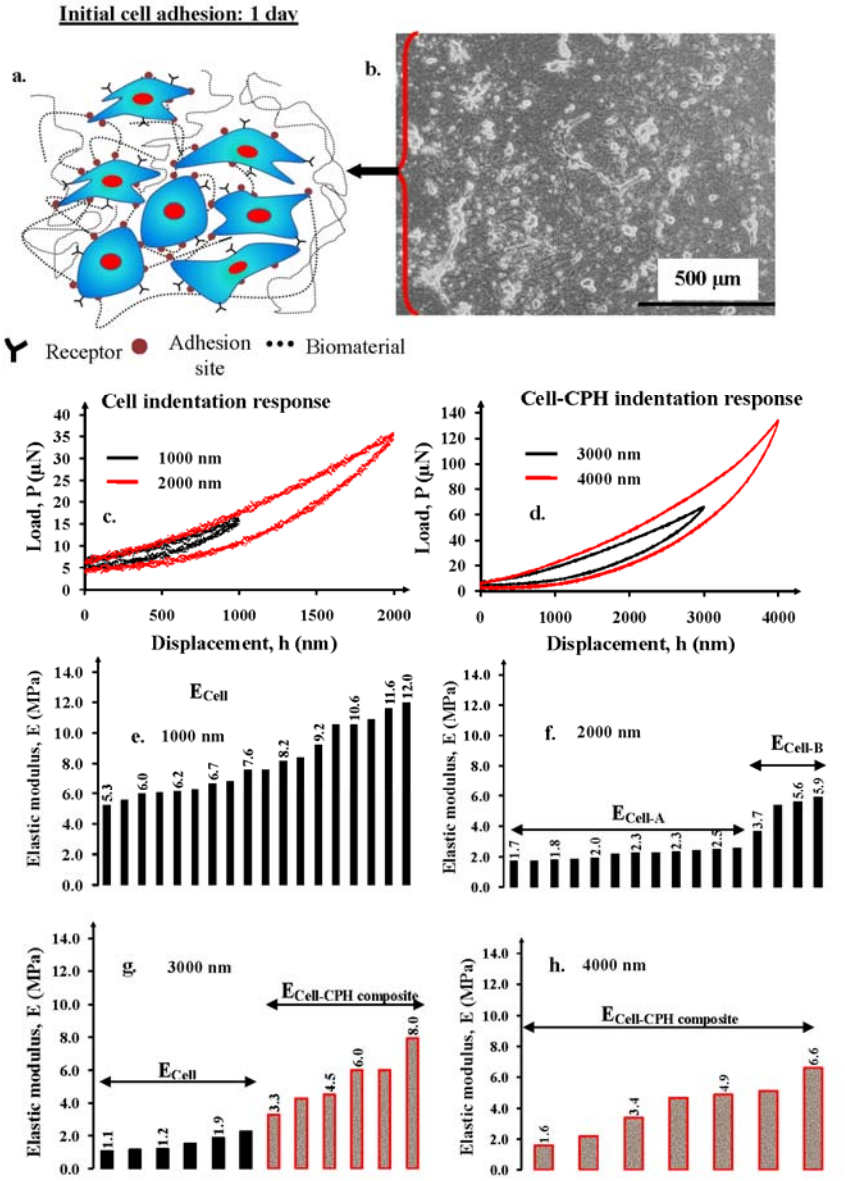

Figure 3: Schematic describes cellular responses during initial cell adhesion (a) as also shown by round cell morphology in optical micrograph (b) taken on 1 day cell seeded CPH film. *In situ* nanomechanical responses of 1 day cultured cells and cell-CPH substrates are obtained (c-h). Mechanical responses of cells and cell-CPH composites are completely reversible as shown by LD curves (c, d). Distinct elastic moduli of cells and cell-substrates are obtained: $E_{Cell,\ 1000\ nm}$ = 5.3-12.0 MPa; $E_{Cell-A,\ 2000\ nm}$ = 1.7-2.5 MPa; $E_{Cell-B,\ 2000\ nm}$ = 3.7-5.9 MPa; $E_{Cell,\ 3000\ nm}$ = 1.1-2.0 MPa; $E_{Cell-CPH\ composite,\ 3000\ nm}$ = 3.3-8.0 MPa; and $E_{Cell-CPH\ composite,\ 4000\ nm}$ = 1.6-6.6 MPa.

are observed over the entire sample surface and some round cells are also observed within the cell clusters. After 4 days of culture, most of the cells are observed to be flat and indentation depths of up to 3000 nm were sufficient to obtain cell-CPH composite indentation responses. LD curves in figures 4c, d indicate that cell and cell-CPH substrate deformations are reversible, and delayed elastic responses are shown by hysteresis in LD curves. After 4 days of culture, steeper loading slopes are observed at 1000 nm & 2000 nm depths (as compared to 1 day cultured cells), which implies a stiff nanomechanical response of flat cells. *In situ* elastic moduli of cells (1000 nm depth), cell-CPH composites (2000 and 3000 nm depth) are plotted in figures 3e-g. *In situ* elastic moduli of 4 days cultured cells and cell-CPH substrates: $E_{Cell,\ 1000\ nm}$ = 4.4-11.0 MPa, $E_{Cell-CPH\ Composite,\ 2000\ nm}$= 3.9-6.3 MPa, and $E_{Cell-CPH\ Composite,\ 3000\ nm}$= 3.7-6.0 MPa.

3.3.3 In situ nanomechanical analysis of cells and cell-CPH after 8 days of culture

A schematic representation of typical cellular responses observed on CPH films demonstrating cell migration and orientation towards core regions indicative of developing bone nodules is shown in Figure 5a. Optical micrograph (figure 5b) taken on 8 days cell-seeded CPH substrate reveals large assembly of cells oriented towards the dense core region. In this micrograph, most of the cells appear to be flat and a few round cells are also observed. The L-D responses of 8 days cultured cells were observed to be similar to those obtained after 1 and 4 days of culture. Some unique load-deformation responses were obtained on core dense regions at indentation depths of 1000, 2000, 3000, 4000 nm, respectively, as shown in figures 5c, d. The L-D curves show stiffer mechanical response of living/nonliving constituents of developing bone nodule, not observed in samples with 1 and 4 days of culture. Large deformations (up to 4000 nm) were applied on core regions to obtain indentation responses from varying depths within the dense regions and obtain multi-layer responses from cell-developing bone nodule-CPH-TCPS substrates (figure 5d). As shown in figure 5d, high loads (1400 μN) are measured beyond 2700 nm depth, which suggest that indentation response is primarily dominated by influence of the stiff TCPS substrate underneath the CPH film. Figures 5e-g show the *in situ* elastic moduli of live cells, developing bone nodules (dense regions), and cell-CPH composites obtained on 8 days cell-seeded CPH films at indentation depths of 1000 nm (figure 5e), 2000 nm (figure 5f), and 3000 nm (figure 5g), respectively. *In situ* elastic moduli of 8 days cultured cells, developing bone nodules and cell-CPH substrates are: 5.7-8.1 MPa at 1000 nm ($E_{Cell,\ 1000\ nm}$), and 29.2-35.5 MPa ($E_{Developing\ bonenodule,\ 1000\ nm}$). 1.6-3.6 MPa for the cell at 2000 nm ($E_{Cell,\ 2000\ nm}$), 59.8-74.4 MPa for developing nodule at 2000

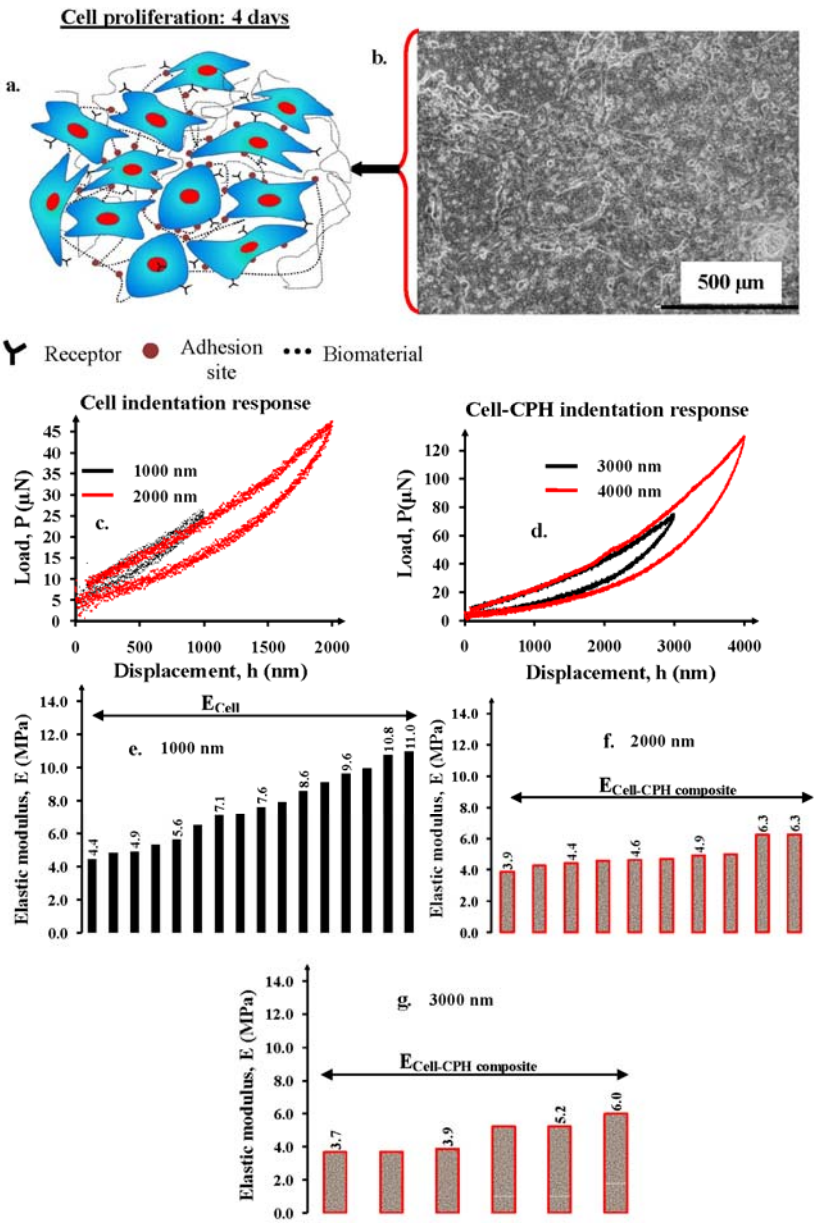

Figure 4: Schematic demonstrates the typical cellular responses such as cell spreading, physical interactions between neighboring cells as shown by corresponding optical micrograph (b) taken after 4 days of culture on cell-seeded CPH films. Flat and round cells and cell clusters are observed all over the sample surface. In situ nanomechanical responses of 4 days cultured cells and cell-CPH substrates are obtained (c-g). LD curves show completely reversible cell deformation of cells and cell-CPH composites. Distinct elastic moduli of cells and cell-substrates are obtained: $E_{Cell,\ 1000\ nm}$ = 4.4-11.0 MPa; $E_{Cell-CPH\ Composite,\ 2000\ nm}$ = 3.9-6.3 MPa; and $E_{Cell-CPH\ Composite,\ 3000\ nm}$ = 3.7-6.0 MPa.

nm ($E_{Developing\ bone\ nodule,\ 2000\ nm}$), 45.5-69.1 MPa for developing bone nodule at 3000 nm($E_{Developing\ bone\ nodule,\ 3000\ nm}$) and 3.7-9.2 MPa for the cell-CPH composite at 3000 nm, ($E_{Cell-CPH\ composite,\ 3000\ nm}$) and 92.7-194.5 MPa for the cell-CPH-TCPS composite response ($E_{Cell-CPH-TCPS\ composite,\ 3000\ nm}$) at 3000 nm.

3.3.4 In situ nanomechanical analyses of bone nodules after 22 days of culture

In vitro bone nodules were observed on CPH films after 22 days of culture. These experiments did not utilize differentiating media. Figure 6a shows the AFM height image revealing a cylindrical orientation of collagen fibers ($\sim$1.7μm). Mineral deposits of various sizes in the nm-μm range are observed to overlay the surface of bone nodule as shown in AFM height image (figure 6b). Optical micrograph (figure 6c) reveals a round dense feature ($\sim$500μm) that has been confirmed to be bone nodule using Alizarin Red S staining and structural-chemical analyses as reported previously (Verma et al. 2010). L-D curve obtained at 1000 nm depth (figure 6d) indicates a stiff nanomechanical response of bone nodule constituents as compared to cells. The L-D curve obtained at 2000 nm depth (figure 6e) shows gradual steps ($\sim$300-400 nm wide) with change in slope in loading portion of the curve. These slope changes and steps are representative of the multiphase characteristics of the bone nodule consisting of tissue and mineralized structures. *In situ* elastic moduli of bone nodule are plotted separately for indentation depths of 1000 nm (figure 6f) and 2000 nm (figure 6g), respectively. A larger range of values of elastic moduli ($E_{Bonenodule,\ 1000\ nm}$=5.5-48.7 MPa and $E_{Bone\ nodule,\ 2000\ nm}$=8.0-21.7 MPa) is observed which can be expected from varying elastic properties of bone nodule constituents such as soft collagenous phases (collagen fibers, fibrils) and stiff hydroxyapatite particles present at different length scales.

4 Discussion

Experiments reported in this work indicate that over the time scale of initial cell adhesion and proliferation, nanomechanical properties of cells fall in the same order of magnitude as that of soaked CPH substrate. With further increase in cell culture duration, cells start synthesizing bone nodules consisting of robust hierarchical structures of collagen and hydroxyapatite that result in stiffer nanomechanical response and elastic moduli measured over 22 days of culture. Further, consistent elastic moduli of soaked CPH films are obtained over 22 days of soaking which suggests that CPH substrates provide sufficient mechanical support to growing cells and bone nodules.

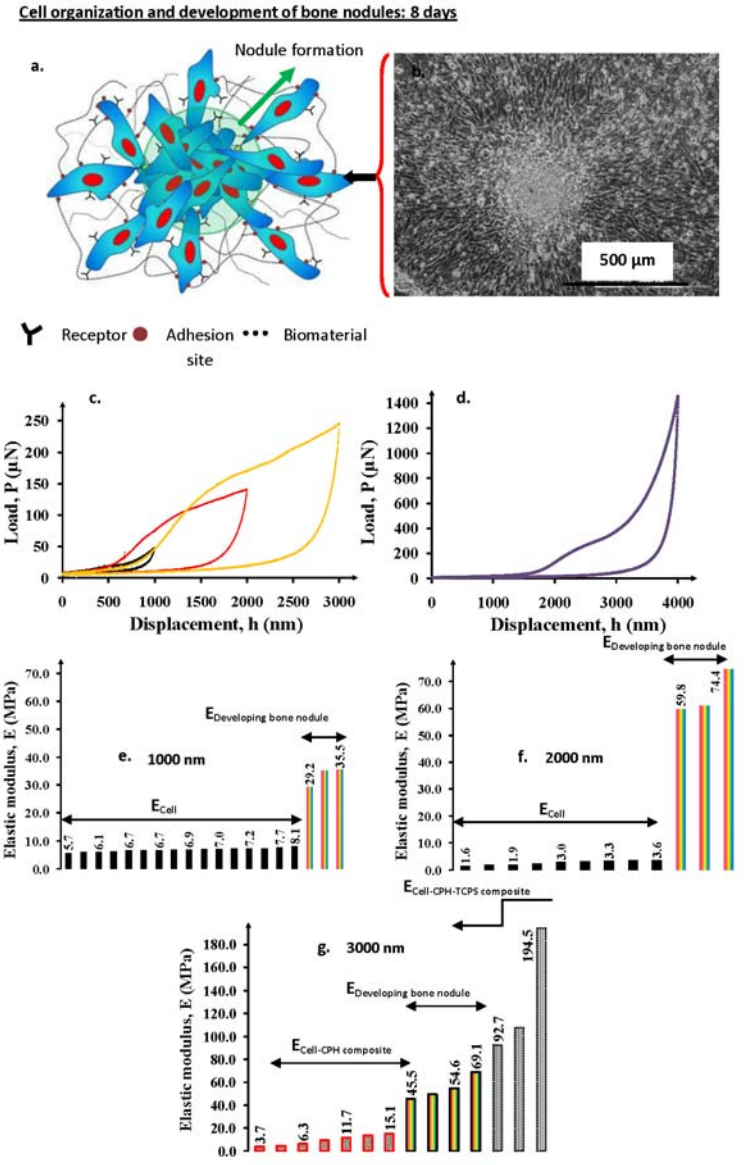

Figure 5: Schematic describes the typical demonstration of cell organization and orientation toward core regions (a) as also observed by optical micrograph (b) after 8 days of culture on cell-seeded CPH films. Stiffer nanomechanical responses of developing bone nodules are shown by steeper loading curves at 1000, 2000 and 3000 nm, respectively. Elastic moduli of cells, developing bone nodules and cell-substrates are obtained: $E_{Cell,1000nm}$ = 5.7-8.1 MPa; $E_{developing\ bone\ nodule,\ 1000\ nm}$ = 29.2-35.5 MPa; $E_{Cell,\ 2000\ nm}$ = 1.6-3.6 MPa; $E_{developing\ bone\ nodule,\ 2000\ nm}$ = 59.8-74.4 MPa; $E_{developing\ bone\ nodule,\ 3000\ nm}$ = 45.5-69.1 MPa; $E_{Cell-CPH\ composite,\ 3000\ nm}$ = 3.7-15.1 MPa and $E_{Cell-CPH-TCPS\ composite,\ 3000\ nm}$ = 92.7-194.5 MPa.

4.1 Cellular responses to swelling of CPH films over duration of 22 days: AFM topography

Physical characteristics of biomaterials are modified as a result of degradation that is likely to influence interactions between cells and biomaterials. Using AFM imaging on cell-seeded CPH films, changes in substrate topography (sectional analysis; figures 2b, e, and f) are observed during 2 days of culture as a result of change in swelling characteristics of CPH films, as reported previously (Khanna et al. 2010). Topographical changes in cell shape, and extension of filapodia over several μm are typical cellular responses to swelling of CPH films (as shown in figure 2) and cells appear to take the shape of swelling substrate. On taking a critical look at shape, size and long extensions of filapodia (figure 2g), it appears that focal adhesions are continuously varying and mechanosensitive and modulate their shapes, sizes and orientations in a response to change in substrate topography/stiffness. These results suggest that cells can sense and respond to substrate swelling thereby exhibiting dynamic physical interactions with the swelling substrate. Overall, CPH films exhibit swelling characteristics, but severe degradation was not observed until 48 days soaking in cell culture medium. Earlier, chitin based biomaterials substrates have been shown to undergo lysozyme based enzymatic degradation. These findings reach to an important conclusion that CPH films were in-tact and provided sufficient physical support for cell adhesion, proliferation and development of hierarchically-organized bone nodules.

4.2 In situ load-deformation behavior of cells and cell-CPH composites

Depending on the amount of strain applied and timescale probed, the osteoblast cells show both elastic and viscoelastic behavior. Nanomechanical properties of cells measured with nanosized probes at smaller depths indicate the elastic deformation of cellular structures such as membranes, cytoskeleton and organelles present near the cell surface. Cytoskeleton provides structural integrity to cell and is known to be inherently viscoelastic and shows frequency or time dependent deformation. (Balland et al. 2006) The soft glassy model predicts that cytoskeleton shows elastic recovery over a time scale of seconds, (Solon et al. 2007) and viscoelastic effects are more likely to occur at longer duration deformation of cell which can be caused by both viscous flow and active remodeling. (Mahaffy et al. 2004) Viscoelastic behavior of materials and biological cells has been widely reported using indentation methods. (Arfsten et al. 2008; Darling et al. 2008; Mahaffy et al. 2004; Park et al. 2009) In this work, indentation tests are performed at depths of 1000 nm, 2000 nm, 3000 nm, and 4000 nm at loading and unloading rate of 100 nm/s for total duration of 20s, 40s, 60s, and 80 s, respectively. Smaller hysteresis observed (figures 3 and 4) at smaller indentation depths display mini-

mal effect of time-dependent mechanical response that may arise from the cellular structures (mainly, cytoskeleton) present near the cell periphery. Large hysteresis in LD cycles (figures 5 and 6) displays distinct time-dependent behavior arising from within cells, bone nodules and swollen CPH films that can be expected under high loading/strain conditions for longer duration tests

4.3 In situ mechanical behavior of cells, bone nodules and cell-CPH composites

Over time, a series of progressive cellular processes are observed such as initial cell adhesion, cell clustering and cell migration and formation dense cell masses (figures 2-6), that may also contribute to dynamic mechanical behavior of cells on CPH substrates. Stiffer nanomechanical responses (as shown in figure 4c) are generally observed from flat cells as compared to round cells, which can be related to cytoskeleton organization. Bone nodules formed on CPH films exhibits hierarchical structures of collagen and hydroxyapatite and may also contain cells embedded within them. Varying load-deformation characteristics and mechanical properties of bone nodules (figure 6) suggests that indentation response arises from individual constituents of bone nodules containing living (embedded cells) and non-living materials (proteins and minerals). Composite mechanical behavior of bone nodule measured at higher indentation depths of 2000 nm, indicates lower spread in elastic moduli. It is interesting to note that hydroxyapatite clusters much larger than a few nanometers are observed much prior to the establishment of fully mineralized bone tissue as seen in figure 6. Such large clusters have also been described in several theoretical and computational studies to play an important role for the elastic and inelastic behavior of bone tissues (Crolet et al. 1993; Eberhardsteiner et al. 2012; Fritsch & Hellmich 2007; Fritsch et al. 2009; Hellmich et al. 2004; Katti et al. 2010a; Pidaparti et al. 1996). The experimental evidence presented also provides input to development bone fibril models through computational approaches .( ) (Pradhan et al. 2012; Pradhan et al. 2011).

In general, elastic moduli of both cells and cell-CPH composites decreased with an increase in indentation depth. Variation in elastic properties of cell-CPH composites may be due to multilayer types of mechanical responses obtained from various regions of cell bodies and swollen CPH films, depending on position of indenter tip on cell-CPH construct. In addition, both cells and swollen CPH films possess varying degrees of time-dependent deformation behavior due to inherent differences in viscoelasticity of cell and swollen CPH film arising from their inherent physical/biological characteristics All of these factors may contribute to spread in elastic moduli of cell-CPH composites i.e. $E_{Cell-CPH\ composite,\ 3000nm,\ 1\ day}$= 3.3-8.0 MPa, $E_{Cell-CPH\ Composite,\ 3000\ nm,\ 4\ days}$= 3.7-6.0 MPa and $E_{Cell-CPHcomposite,\ 3000nm,\ 8\ days}$=

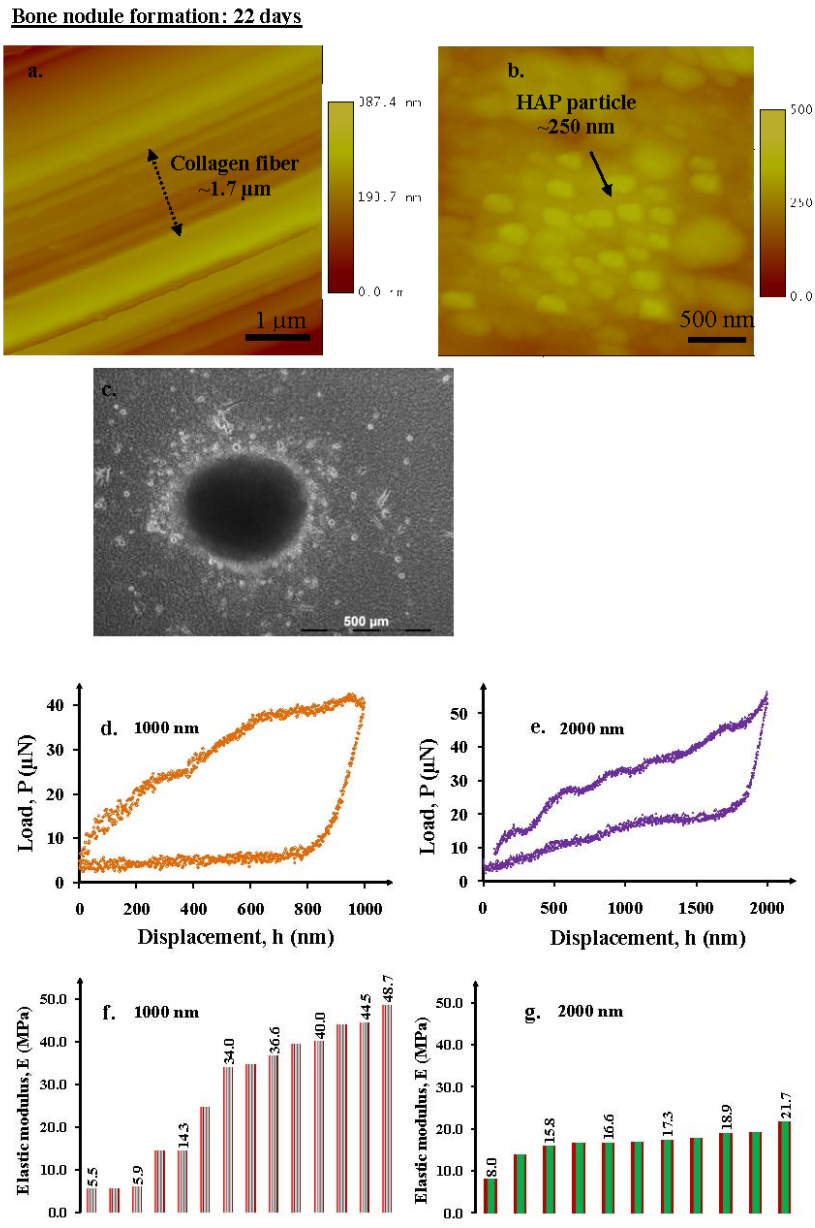

Figure 6: AFM height images showing the collagen fibers (∼1.7 μm diameter) (a) and HAP particles (∼250 nm) (b) present on the bone nodules after 22 days of culture. (c). Load-deformation behavior of bone nodules at indentation depths of 1000 nm (d) and 2000 nm (e), respectively. Elastic moduli of bone nodule constituents are: $E_{Bonenodule,\ 1000\ nm}$ =5.5-48.7 MPa and $E_{Bonenodule,\ 2000\ nm}$ =8.0-21.7 MPa.

3.7-9.2 MPa. Elastic properties of cell-CPH did not change significantly over time, suggesting that interactions between cells and CPH films were maintained over time. Over 22 days, composite responses of bone nodule and CPH film substrate were difficult to measure due to large thickness of bone nodules ($\sim$1-2 mm) and limitation with the maximum displacement limit (5 μm) that can be obtained with nanoindentation instrument.

5 Conclusions

1. Here we present a novel *in situ* nanoindentation experiment developed to evaluate the mechanical behavior of live osteoblasts, developing and mature bone nodules and cell-biomaterial interfaces for tissue engineering applications. Overall, the CPH substrates provide favorable microenvironment for cell organization and bone nodule generation and in-turn regulate the mechanical behavior of cell-substrate interactions for bone regeneration.

2. Over the time scale of cell adhesion, proliferation and bone nodule regeneration (22 days), changes in mechanical behavior of cells are seen as shown by elastic properties of cells with flat cells (4 days) indicating higher stiffness In situ Mechanical Response of Human Osteoblasts on Chitosan-Polygalacturonic acid-Hydroxyapatite Nanocomposites than round (1 day) and oriented cells (8 days), respectively.

3. Consistent range of elastic properties of cell-CPH composites were measured ($E_{Cell-CPH\ composite,\ 3000\ nm,\ 1\ day}$= 3.3-8.0 MPa, $E_{Cell-CPH,3000nm,4days,}$= 3.7-6.0 MPa and $E_{Cell-CPHcomposite,\ 3000\ nm,\ 8\ days}$= 3.7-9.2 MPa) which reaches to an important conclusion that interactions between cells and CPH films at cell-CPH interfaces were maintained.

4. Cells can feel and respond to swelling of CPH films by modulating their shape and focal adhesions as revealed by AFM topographic images on cells.

5. Overall, elastic moduli of cells and bone nodules fall in the same order of magnitude as that of swelling CPH films (i.e. in MPa). These results suggest that tissue engineered substrates such as CPH films may not need to possess the bone-like stiffness of the order of GPa for bone nodule regeneration.

Hence, the deformation behavior of cells is observed to be different on synthetic biodegradable CPH films than that on TCPS substrates. We have observed substrate stiffness dependent differences between response of cells on TCPS and CPH films i.e. elastic properties of cells cultured on CPH films (E$\sim$5-12 MPa) match closely with that of soaked CPH substrates (E$\sim$10-20 MPa) and bone nodules are formed

on CPH films. These results suggests that cells may get stimulated by substrate of matching stiffness (CPH film) and start organizing themselves to develop their own extracellular matrix. This further suggests that physico-chemical-mechanical characteristics of biodegradable CPH substrates provide favorable microenvironment for tissue regeneration which in turn regulates the mechanical behavior of cell-substrate interactions.

In this work, *in situ* nanomechanical behavior of cells, bone nodules and cell-CPH composites have been evaluated. Adopting this methodology, cell-substrate interactions can be modulated by tuning the material properties so as to provide the optimal template for cells for bone regeneration.∼Nanomechanical analyses on biological and biodegradable materials presented in this work are applicable in diverse areas of tissue engineering which employs the use of nanoindentaion as an effective mechanical property measurement technique for studying the multiscale experimental mechanics of cells-tissue-material systems over the time scale of tissue generation These studies provide valuable input and also insight into development of multiscale models of fibrillar and higher lever models of bone. Design of scaffold systems for tissue regeneration is expected to be greatly enhanced with computational techniques that predict the time evolution of scaffold mechanics. It is very useful to have nanomechanical data of elastic behavior of cells and tissues during bone generation available for the development of robust computational models.

Acknowledgement: Authors would like to acknowledge support from ND EPSCoR for tissue culture laboratory facilities. Additionally, author RK would like to acknowledge assistantship from NDSU graduate school. The nanoindentation and atomic force microscopy equipment used was obtained through NSF Instrumentation for Materials Research grant.

References

Abrahamsson, C. K.; F. Yang, H. Park, J. M. Brunger, P. K. Valonen, R. Langer, J. F. Welter, A. I. Caplan, F. Guilak, L. E. Freed. (2010): Chondrogenesis and Mineralization During In Vitro Culture of Human Mesenchymal Stem Cells on Three-Dimensional Woven Scaffolds. *Tissue Engineering Part A*, vol. 16, pp. 3709-3718.

Ahearne, M.; Y. Yang, A. J. El Haj, K. Y. Then, K. K. Liu. (2005): Characterizing the viscoelastic properties of thin hydrogel-based constructs for tissue engineering applications. *Journal of the Royal Society Interface*, vol. 2, pp. 455-463.

Allan S H. (2002): Hydrogels for biomedical applications. *Advanced Drug Delivery Reviews*, 54, pp. 3-12.

Ambre, A.; K. S. Katti, D. R. Katti. (2011): In situ mineralized hydroxyapatite on amino acid modified nanoclays as novel bone biomaterials. *Materials Science & Engineering C-Materials for Biological Applications*, vol. 31, pp. 1017-1029.

Arfsten, J.; C. Bradtmöller, I. Kampen, A. Kwade. (2008): Compressive testing of single yeast cells in liquid environment using a nanoindentation system. *Journal of Materials Research*, vol. 23, pp. 3153-3160.

Balland, M.; N. Desprat, D. Icard, S. Féréol, A. Asnacios, J. Browaeys, S. Hénon, F. Gallet. (2006): Power laws in microrheology experiments on living cells: Comparative analysis and modeling. *Physical Review E*, vol. 74, pp. 021911.

Balooch, G.; G. W. Marshall, S. J. Marshall, O. L. Warren, S. A. S. Asif, M. Balooch. (2004): Evaluation of a new modulus mapping technique to investigate microstructural features of human teeth. *Journal of Biomechanics*, vol. 37, pp. 1223-1232.

Balooch, M.; S. Habelitz, J. H. Kinney, S. J. Marshall, G. W. Marshall. (2008): Mechanical properties of mineralized collagen fibrils as influenced by demineralization. *Journal of Structural Biology*, vol. 162, pp. 404-410.

Banwell, E. F.; E. S. Abelardo, D. J. Adams, M. A. Birchall, A. Corrigan, A. M. Donald, M. Kirkland, L. C. Serpell, M. F. Butler, and D. N. Woolfson. (2009): Rational design and application of responsive [alpha]-helical peptide hydrogels. *Nat Mater*, vol. 8, pp. 596-600.

Basu, S.; and M. W. Barsoum. (2007): Deformation micromechanisms of ZnO single crystals as determined from spherical nanoindentation stress–strain curves. *Journal of Materials Research*, vol. 22, pp. 2470-2477.

Crolet, J. M., B. Aoubiza, A. Meunier. (1993): Compact-bone - numerical-simulation of mechanical characteristics. *Journal of Biomechanic, vol.* 26, pp.:677-687.

Darling, E. M.; M. Topel, S. Zauscher, T. P. Vail, F. Guilak. (2008): Viscoelastic properties of human mesenchymally-derived stem cells and primary osteoblasts, chondrocytes, and adipocytes. *Journal of biomechanics*, 41, pp. 454-464.

Discher, D. E.; D. J. Mooney, P. W. Zandstra. (2009): Growth Factors, Matrices, and Forces Combine and Control Stem Cells. *Science*, vol. 324:1673-1677.

Du, Y.; E. Lo, S. Ali, A. Khademhosseini. (2008): Directed assembly of cell-laden microgels for fabrication of 3D tissue constructs. *Proceedings of the National Academy of Sciences*, vol. 105, pp. 9522-9527.

Ebenstein, D. M.; and L. A. Pruitt. (2004): Nanoindentation of soft hydrated

materials for application to vascular tissues. *Journal of Biomedical Materials Research Part A*, vol. 69A, pp. 222-232.

Eberhardsteiner, L., C. Hellmich, S. Schiener. (2012): Layered water in crystal interfaces as source for bone viscoelasticity: arguments from a multiscale approach. *Computer Methods in Biomechanics and Biomedical Engineering* doi 10.1080/10255842.2012.670227.

Ebenstein, D. M.; and L. A. Pruitt. 2006. Nanoindentation of biological materials. *Nano Today*, vol. 1, pp. 26-33.

Engelmayr, G. C.; M. Cheng, C. J. Bettinger, J. T. Borenstein, R. Langer, L. E. Freed. (2008): Accordion-like honeycombs for tissue engineering of cardiac anisotropy. *Nat Mater*, vol. 7, pp. 1003-1010.

Freed, L. E.; G. C. Engelmayr, J. T. Borenstein, F. T. Moutos, and F. Guilak. (2009): Advanced Material Strategies for Tissue Engineering Scaffolds. *Advanced Materials*, vol. 21, pp. 3410-3418.

Fritsch, A., C. Hellmich. (2007): 'Universal' microstructural patterns in cortical and trabecular, extracellular and extravascular bone materials: Micromechanics-based prediction of anisotropic elasticity. *Journal of Theoretical Biology, vol.* 244, pp. 597-620.

Fritsch, A., C. Hellmich, L. Dormieux. (2009): Ductile sliding between mineral crystals followed by rupture of collagen crosslinks: Experimentally supported micromechanical explanation of bone strength. *Journal of Theoretical Biology*, vol. 260, pp. 230-252.

Gaharwar, A. K.; S. A. Dammu, J. M. Canter, C.-J. Wu, G. Schmidt. (2011): Highly Extensible, Tough, and Elastomeric Nanocomposite Hydrogels from Poly(ethylene glycol) and Hydroxyapatite Nanoparticles. *Biomacromolecules*, vol. 12, pp. 1641-1650.

Gkioni, K.; S. C. G. Leeuwenburgh, T. E. L. Douglas, A. G. Mikos, and J. A. Jansen. (2010): Mineralization of Hydrogels for Bone Regeneration. *Tissue Engineering Part B: Reviews*, vol. 16, pp. 577-585.

Guilak, F.; D. M. Cohen, B. T. Estes, J. M. Gimble, W. Liedtke, and C. S. Chen. (2009): Control of Stem Cell Fate by Physical Interactions with the Extracellular Matrix. *Cell stem cell*, vol. 5, pp. 17-26.

Hellmich, C., J. F. Barthelemy, L. Dormieux. (2004): Mineral-collagen interactions in elasticity of bone ultrastructure - a continuum micromechanics approach. *European Journal of Mechanics a-Solids* , vol. 23, pp. 783-810.

Ingber, D. E. (2003): Mechanobiology and diseases of mechanotransduction. Annals of Medicine vol. 35, pp. 564-577.

Katti, D. R., S. M. Pradhan, K. S. Katti. (2010a): Directional dependence of hydroxyapatite-collagen interactions on mechanics of collagen. *Journal of Biomechanics, vol. 43*, pp. 1723-1730.

Katti, K. S.; A. H. Ambre, N. Peterka, D. R. Katti. (2010): Use of unnatural amino acids for design of novel organomodified clays as components of nanocomposite biomaterials. *Philosophical Transactions of the Royal Society a-Mathematical Physical and Engineering Sciences*, vol. 368, pp. 1963-1980.

Katti, K. S.; B. Mohanty, D. R. Katti. (2006a): Nanomechanical properties of nacre. *Journal of Materials Research*, vol. 21, pp. 1237-1242.

Katti, K. S.; P. Turlapati, D. Verma, R. Bhowmik, P. K. Gujjula, and D. R. Katti. (2006b): Static and dynamic mechanical behavior of hydroxyapatite-polyacrylic acid composites under simulated body fluid. *American Journal of Biochemistry and Biotechnology*, vol. 2, pp. 73-79.

Katti, K. S.; P. Turlapati, D. Verma, R. Bhowmik, P. K. Gujjula, and D. R. Katti. (2006c): Static and Dynamic Mechanical Behavior of Hydroxyapatite-Polyacrylic Acid Composites Under Simulated Body Fluid. *American Journal of Biochemistry and Biotechnology*, vol. 2 (2), pp. 73-79,.

Khanna, R.; D. R. Katti, K. S. Katti. (2011a): Experiments in Nanomechanical properties of Live Osteoblast Cells and cell-Biomaterial Interface. *ASME Journal of nanotechnology for engineering and medicine to appear*.

Khanna, R.; K. S. Katti, D. R. Katti. (2009): Nanomechanics of Surface Modified Nanohydroxyapatite Particulates Used in Biomaterials. *Journal of Engineering Mechanics-Asce*, vol. 135, pp. 468-478.

Khanna, R.; K. S. Katti, D. R. Katti. (2010): In Situ Swelling Behavior of Chitosan-Polygalacturonic Acid/Hydroxyapatite Nanocomposites in Cell Culture Media. International *Journal of Polymer Science*, vol. 2010, Article ID 175264.

Khanna, R.; K. S. Katti, D. R. Katti. (2011b): Bone nodules on chitosan-polygalacturonic acid-hydroxyapatite nanocomposite films mimic hierarchy of natural bone. *Acta Biomaterialia*, vol. 7, pp. 1173-1183.

Kinney, J. H.; S. J. Marshall, G. W. Marshall. 2003: The Mechanical Properties of Human Dentin: a Critical Review and Re-evaluation of the Dental Literature. *Critical Reviews in Oral Biology & Medicine*, vol. 14, pp. 13-29.

Langer, R.; and J. P. Vacanti. 1993: Tissue Engineering. *Science*, vol. 260, pp. 920-926.

Lutolf, M. P.; and J. A. Hubbell. (2005): Synthetic biomaterials as instructive extracellular microenvironments for morphogenesis in tissue engineering. *Nature Biotechnology*, vol. 23, pp. 47-55.

Mahaffy, R. E.; S. Park, E. Gerde, J. Käs, C. K. Shih. (2004): Quantitative Analysis of the Viscoelastic Properties of Thin Regions of Fibroblasts Using Atomic Force Microscopy. *Biophysical journal*, vol. 86, pp. 1777-1793.

Mashmoushy, H.; Z. Zhang, C. R. Thomas. (1998): Micromanipulation measurement of the mechanical properties of baker's yeast cells. *Biotechnology Techniques*, vol. 12, pp. 925-929.

Mohanty, B.; K. S. Katti, D. R. Katti, D. Verma. (2006): Dynamic nanomechanical response of nacre. *Journal of Materials Research*, vol. 21, pp. 2045-2051.

Ng, L.; H.-H. Hung, A. Sprunt, S. Chubinskaya, C. Ortiz, and A. Grodzinsky. (2007): Nanomechanical properties of individual chondrocytes and their developing growth factor-stimulated pericellular matrix. *Journal of Biomechanics*, vol. 40, pp. 1011-1023.

Nudelman, F.; K. Pieterse, A. George, P. H. Bomans, H. Friedrich, L. J. Brylka, P. A. Hilbers, G. de With, N. A. Sommerdijk. (2010): The role of collagen in bone apatite formation in the presence of hydroxyapatite nucleation inhibitors. *Nat Mater*, vol. 9, pp. 1004-1009.

Oliver, W. C.; and G. M. Pharr. (1992): An improved technique for determining hardness and elastic-modulus using load and displacement sensing indentation experiments. *Journal of Materials Research*, vol. 7, pp. 1564-1583.

Oliver, W. C.; and G. M. Pharr. (2004): Measurement of hardness and elastic modulus by instrumented indentation: Advances in understanding and refinements to methodology. *Journal of Materials Research*, vol. 19, pp. 3-20.

Oliver, W. C.; and G. M. Pharr. (2010): Nanoindentation in materials research: Past, present, future. *Mrs Bulletin*, vol. 35, pp. 897-907.

Pagliari, S.; A. C. Vilela-Silva, G. Forte, F. Pagliari, C. Mandoli, G. Vozzi, S. Pietronave, M. Prat, S. Licoccia, A. Ahluwalia, E. Traversa, M. Minieri, P. Di Nardo. (2011): Cooperation of Biological and Mechanical Signals in Cardiac Progenitor Cell Differentiation. *Advanced Materials*, vol. 23, pp. 514-518.

Park, S.; K. D. Costa, G. A. Ateshian, K.-S. Hong. (2009): Mechanical properties of bovine articular cartilage under microscale indentation loading from atomic force microscopy. *Proceedings of the Institution of Mechanical Engineers, Part H: Journal of Engineering in Medicine*, vol. 223, pp. 339-347.

Pharr, G. M.; and W. C. Oliver. (1992). Measurement of thin-film mechanical-properties using nanoindentation. *Mrs Bulletin*, vol. 17, pp. 28-33.

Pidaparti, R. M. V., A. Chandran, Y. Takano, C. H. Turner. (1996)): Bone mineral lies mainly outside collagen fibrils: Predictions of a composite model for osteonal bone. *Journal of Biomechanics* , vol. 29, pp. 909-916.

Pradhan, S., M., K. Katti, S., K. Katti, S. (2012): A Multiscale Model of Collagen Fibril In Bone: Elastic Response. *ASCE J. of Engineering Mechanics* in press.

Pradhan, S. M., D. R. Katti, k. S. Katti. (2011): Steered Molecular Dynamics Study of Mechanical Response of Full Length and Short Collagen Molecules. *Journal of Nanomechanics and Micromechanics, vol.* 1, pp. 104-110.

Rezwan, K.; Q. Z. Chen, J. J. Blaker, A. R. Boccaccini. (2006): Biodegradable and bioactive porous polymer/inorganic composite scaffolds for bone tissue engineering. *Biomaterials*, vol. 27, pp. 3413-3431.

Rho, J.-Y.; M. E. Roy, T. Y. Tsui, G. M. Pharr. (1999): Elastic properties of microstructural components of human bone tissue as measured by nanoindentation. *Journal of Biomedical Materials Research*, vol. 45, pp. 48-54.

Roy, M. E.; J.-Y. Rho, T. Y. Tsui, N. D. Evans, G. M. Pharr. (1999): Mechanical and morphological variation of the human lumbar vertebral cortical and trabecular bone. Journal of *Biomedical Materials Research*, vol. 44, pp. 191-197.

Saha, R.; and W. D. Nix. (2002): Effects of the substrate on the determination of thin film mechanical properties by nanoindentation. *Acta Materialia*, vol. 50, pp. 23-38.

Slaughter, B. V.; S. S. Khurshid, O. Z. Fisher, A. Khademhosseini, and N. A. Peppas. (2009): Hydrogels in Regenerative Medicine. *Advanced Materials*, vol. 21, pp. 3307-3329.

Solon, J.; I. Levental, K. Sengupta, P. C. Georges, P. A. Janmey. (2007): Fibroblast Adaptation and Stiffness Matching to Soft Elastic Substrates. *Biophysical Journal*, vol. 93, pp. 4453-4461.

Subra, S. (2007): Biomechanics and biophysics of cancer cells. *Acta Biomaterialia*, vol. 3, pp. 413-438.

Tai, K.; G. Pelled, D. Sheyn, A. Bershteyn, L. Han, I. Kallai, Y. Zilberman, C. Ortiz, D. Gazit. (2008): Nanobiomechanics of Repair Bone Regenerated by Genetically Modified Mesenchymal Stem Cells. *Tissue Engineering Part A*, vol. 14, pp. 1709-1720.

Van Vliet, K. J.; G. Bao, S. Suresh. (2003). The biomechanics toolbox: experimental approaches for living cells and biomolecules. *Acta Materialia*, vol. 51, pp. 5881-5905.

Verma, D.; K. Katti, D. Katti. (2006a): Bioactivity in in situ hydroxyapatite-polycaprolactone composites. *Journal of Biomedical Materials Research Part A*, vol. 78A, pp. 772-780.

Verma, D.; K. Katti, D. Katti. (2006b): Experimental investigation of interfaces in hydroxyapatite/polyacrylic acid/polycaprolactone composites using photoacous-

tic FTIR spectroscopy. *Journal of Biomedical Materials Research Part A*, vol. 77A, pp. 59-66.

Verma, D.; K. S. Katti, D. R. Katti. (2008a): Effect of biopolymers on structure of hydroxyapatite and interfacial interactions in biomimetically synthesized hydroxyapatite/biopolymer nanocomposites. *Annals of Biomedical Engineering*, vol. 36, pp. 1024-1032.

Verma, D.; K. S. Katti, D. R. Katti. (2009): Polyelectrolyte-complex nanostructured fibrous scaffolds for tissue engineering. *Materials Science & Engineering C-Materials for Biological Applications*, vol. 29, pp. 2079-2084.

Verma, D.; K. S. Katti, D. R. Katti. (2010): Osteoblast adhesion, proliferation and growth on polyelectrolyte complex-hydroxyapatite nanocomposites. *Philosophical Transactions of the Royal Society a-Mathematical Physical and Engineering Sciences*, vol. 368, pp. 2083-2097.

Verma, D.; K. S. Katti, D. R. Katti, B. Mohanty. (2008b): Mechanical response and multilevel structure of biomimetic hydroxyapatite/polygalacturonic/chitosan nanocomposites. *Materials Science & Engineering C-Biomimetic and Supramolecular Systems*, vol. 28, pp. 399-405.

Wang, N.; J. Butler, D. Ingber. (1993): Mechanotransduction across the cell surface and through the cytoskeleton. *Science*, vol. 260, pp. 1124-1127.

Wei, G.; and P. X. Ma. (2008): Nanostructured Biomaterials for Regeneration. *Advanced Functional Materials*, vol. 18, pp. 3568-3582.

Wheeldon, I.; A. F. Ahari, A. Khademhosseini. (2010): Microengineering Hydrogels for Stem Cell Bioengineering and Tissue Regeneration. *Journal of the Association for Laboratory Automation* vol. 15, pp. 440-448.

Yim, E. K. F.; E. M. Darling, K. Kulangara, F. Guilak, K. W. Leong. (2010): Nanotopography-induced changes in focal adhesions, cytoskeletal organization, and mechanical properties of human mesenchymal stem cells. *Biomaterials*, vol. 31, pp. 1299-1306.